Atmospheric Refractivity Corrections in Satellite Laser Ranging

JAMES B. ABSHIRE, SENIOR MEMBER, IEEE, AND CHESTER S. GARDNER, SENIOR MEMBER, IEEE

Abstract—**Atmospheric refraction can cause significant errors in satellite laser ranging (SLR) systems. There are two techniques which can be used to correct for these errors. Atmospheric models based upon surface measurements of pressure, temperature, and relative humidity have been shown by ray tracing to be accurate to within a few centimeters at 20° elevation angle. The residual errors in the models are thought to be primarily caused by horizontal gradients in the refractivity. Although models have been developed to predict the gradient effects, initial studies show that they can be sensitive to local topographic effects. Atmospheric turbulence can introduce random fluctuations in the refractivity, but only introduces centimeter level errors at elevation angles below 10°. Pulsed two-color ranging systems can directly measure the atmospheric delay in satellite ranging. These systems require mode-locked multiple-frequency lasers and streak-camera-based receivers and currently appear capable of measuring the atmospheric delay with an accuracy of 0.5 cm or better.**

I. Introduction

PULSED satellite laser ranging (SLR) systems estimate the distance to retroreflector equipped satellites by measuring the round-trip pulse propagation time. While currently operational SLR systems can measure this time with errors on the order of 150 ps, next generation systems [1] should be capable of to less than 50-ps error. Both atmospheric refraction and turbulence introduce errors into SLR systems. Atmospheric refraction increases the average optical path length to an orbiting satellite by $2\frac{1}{2}$ m when it is near zenith and by more than 13 m when the satellite is at 10° elevation. Strong turbulence can introduce random errors into the optical path length approaching several centimeters at 10° elevation.

Models have been developed to correct SLR measurements for the average atmospheric refractive delay. They utilize atmospheric measurements taken at the ranging site and currently are thought to be accurate to within a few centimeters at 20° elevation. More accurate models can correct for horizontal refractivity gradients as well as for the spherically symmetric refractivity. These more complex models require numerous meteorological measurements which are spatially separated by 10 km or more. Furthermore, models which use only surface measurements can be sensitive to local topography and other effects on the atmosphere near the Earth's surface.

Manuscript received November 1, 1984; revised March 4, 1985. This work was supported in part by the Goddard Director's Discretionary Fund, and in part under NASA Grant NSG-5049.

J. B. Abshire is with the Instrument Electro-Optics Branch, NASA-Goddard Space Flight Center, Greenbelt, MD 20771.

C. S. Gardner is with the Department of Electrical and Computer Engineering, University of Illinois, Urbana, IL 61801.

Two-color ranging systems can directly measure the atmospheric delay by utilizing the dispersion in the atmospheric refraction. For currently available Nd:YAG or Alexandrite lasers, the dispersion is approximately 5–10 percent of the single-color delay. Therefore to measure single-color atmospheric delay to 1 cm, about 1-mm accuracy is required in the dispersion measurement. Hence two-color systems must have very high accuracy in measuring the differential signal transit time.

Due to the large distance in SLR, pulsed two-color systems now seem preferable to continuous wave (CW) techniques. Pulsed two-color systems require both mode-locked multiple-frequency lasers and streak-camera-based receivers for millimeter or submillimeter differential delay measurements. Careful calibration techniques and minicomputer processing are required to optimize the performance of such systems. Based upon recent work, it appears that pulsed two-color systems can measure the single-color atmospheric delay to 0.5 cm or better.

II. Background

The geometry for a laser ranging site and its satellite target is shown in Fig. 1. The optical path length between the site and target is defined as the integral of the group refractive index along the ray path. If the refractivity is spherically symmetric, the ray path will lie entirely in a plane. In this case the apparent range measured by a pulsed laser system is given by

$$R_0 = \int_{r_0}^{r_1} dr \, \frac{n_g}{\sin \theta}. \tag{1}$$

Here n_g is the group index of refraction and θ is given by Snell's law for a spherically stratified medium (see Fig. 1)

$$nr \cos \theta = n_0 r_0 \cos \theta_0 \tag{2}$$

where n_0 is the phase refractive index at the laser site.

The atmospheric correction is the difference between the optical range R_0 and the straight path length R_s. If the group refractive index is expressed in terms of the group refractivity N_g

$$n_g = 1 + 10^{-6} N_g \tag{3}$$

then the atmospheric correction can be expressed as

$$AC = R_0 - R_s = 10^{-6} \int_{r_0}^{r_1} dr \, \frac{Ng}{\sin \theta} + \left[\int_{r_0}^{r_1} \frac{\mathrm{dr}}{\sin \theta} - R_s \right]. \tag{4}$$

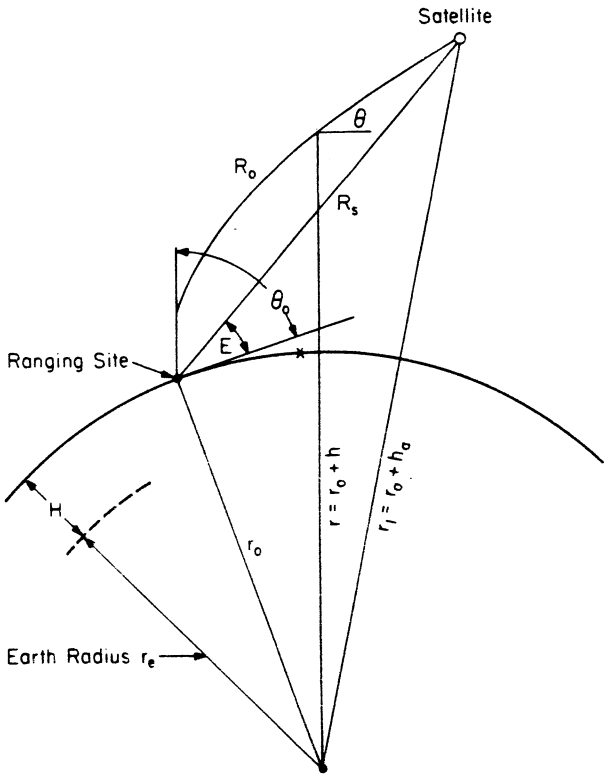

Fig. 1. Geometry of satellite and ground target.

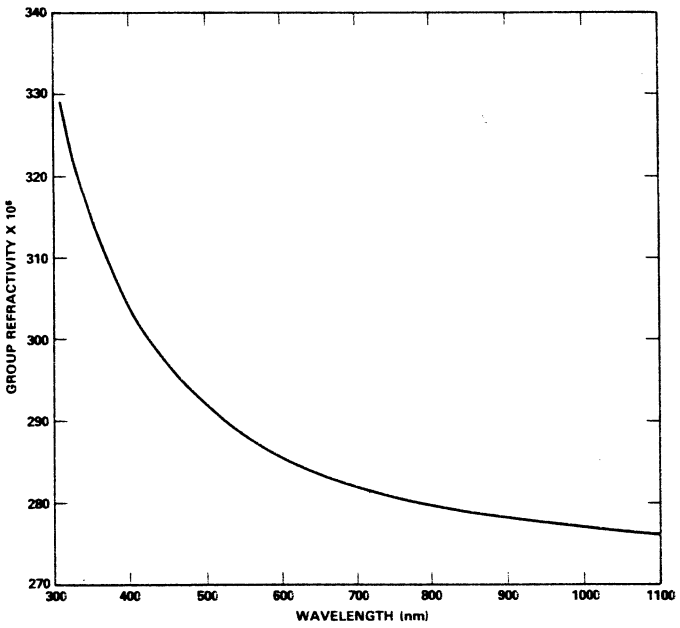

Fig. 2. Group refractivity of air at P = 1013.25 mbar, T = 15°C, and RH = 50 percent.

The first term in (4) is the velocity error, which is dominant, while the bracketed term is the difference between the geometric lengths of the ray and straight-line path. The bracketed term reaches a maximum value of 3–4 cm at 10° elevation and is negligible above 30°. Elevation angles lower than 10–20° are seldom used in operational SLR systems due to increased atmospheric attenuation and site obstructions. However, in practice, the exact cutoff angle depends both upon site geometry and atmospheric conditions.

At optical wavelengths the group refractivity can be expressed as [2]

$$N_g = R_d D_d + R_w D_w \tag{5}$$

where the dry air and water vapor (wet) specific group refraction terms are given by

$$R_d = 23.7134 + 6839.397 \frac{(130 + \sigma^2)}{(130 - \sigma^2)^2} + 45.473 \frac{(38.9 + \sigma^2)}{(38.9 - \sigma^2)^2} \tag{6}$$

$$R_w = 64.8731 + 1.74174\sigma^2 - 3.55750 \times 10^{-2}\sigma^4 + 6.1957 \times 10^{-3}\sigma^6 \tag{7}$$

and the dry and wet density terms are given by

$$D_d = \frac{P_d}{T}\left[1 + P_d\left(57.90 \times 10^{-8} - \frac{9.3250 \times 10^{-4}}{T} + \frac{0.25844}{T^2}\right)\right] \tag{8}$$

$$D_w = \frac{e}{T}\left\{1 + e[1 + 3.7 \times 10^{-4} e] \cdot \left[-2.37321 \times 10^{-2} + \frac{2.23366}{T} - \frac{710.792}{T^2} + \frac{7.75141 \times 10^4}{T^3}\right]\right\}. \tag{9}$$

In this formula, $\sigma = 1/\lambda$ and

P_d is the partial pressure of dry air (mbar),
T is the atmospheric temperature (degrees Kelvin),
e is the partial pressure of water vapor (mbar), and
λ is the optical wavelength (μm).

Marini and Murray[3] have simplified this formula for laser ranging applications to

$$N_g = 80.343 f(\lambda)\,(P/T) - 11.3\,(e/T) \tag{10}$$

where

$$f(\lambda) = 0.9650 + \frac{0.0164}{\lambda^2} + \frac{0.000228}{\lambda^4}.$$

The dispersion factor $f(\lambda)$ accounts for the wavelength variation of N_g. The group refractivity of water vapor, which is significant at microwave frequencies, is typically less than 1 percent of the dry component at optical wavelengths. N_g is plotted versus λ in Fig. 2 for typical atmospheric conditions.

III. Atmospheric Models

Numerous formulas have been developed which can partially correct range measurements for the average effects of atmospheric refraction. Two spherical models which provide accuracies of a few centimeters at 20° elevation were developed by Marini and Murray [3] and Saasta-

moinen [4]. Further improvements in spherical models for low elevation angles (10°-20°) have been discussed recently by Davies *et al.* [5] and Truehaft *et al.* [6]. The limiting error sources in the best spherical models are presently believed to be horizontal gradients in the refractive correction.

A. Model Description

Formulas such as Marini and Murray's are particularly convenient for correcting satellite ranging data because they only require measurements of P, T, and relative humidity (RH) taken at the laser site during the satellite pass. However, their formula was derived by assuming that atmospheric refraction is spherically symmetric. Because this assumption holds only approximately in the troposphere, horizontal refractivity gradients can introduce centimeter-level errors into spherical-correction formulas at low elevation angles. A gradient-correction model [7] based upon surface meteorological measurements has been developed by Gardner to predict this effect.

The general form of the atmospheric models can be expressed by writing the range correction for atmospheric refraction in the form

$$AC = SC + GC. \tag{11}$$

The term SC models the spherically symmetric atmosphere, while the term GC models the horizontal refractivity gradients. The correction terms can be expressed as functions of meteorological parameters by evaluating the integrals in (4) using an appropriate group refractivity profile. This profile can be obtained by using the perfect gas law, the law of partial pressures and the hydrostatic equation. The resulting spherical- and gradient-correction formulas [3], [7] are given by

$$SC = \frac{f(\lambda)}{\mathrm{F}(\theta, H)} \frac{A + B}{\sin E + \dfrac{B/(A + B)}{\sin E + 0.01}} \tag{12}$$

and

$$GC = \frac{C}{\sin E \tan E} \boldsymbol{n} \cdot \nabla (P_s T_s K_s) + \frac{D(1 + 1/2 \cos^4 E)}{\sin^3 E \tan E} \boldsymbol{n} \cdot \nabla \left[\frac{P_s T_s^2 K_s^2}{2 - K_s}\right] \tag{13}$$

where

$$F(\theta, H) = 1 + 0.0026 \cos 2\theta - 0.0031H \tag{14}$$

$$K_s = 1.163 + 0.00968 \cos 2\theta - 0.00104T_s + 0.00001435P_s \tag{15}$$

$$A = 0.002347P_s + 0.00141e_s \tag{16}$$

$$B = (1.084 \times 10^{-8}) P_s T_s K_s + (4.735 \times 10^{-8}) \cdot (P_s^2/T_s) 2(3 - 1/K_s) \tag{17}$$

$$C = 80.343 f(\lambda) \frac{R^2}{(Mg)^2} 10^{-6} = 6.915 \times 10^{-2} f(\lambda) \tag{18}$$

$$D = -80.343 f(\lambda) \frac{2}{r_0} \frac{R^3}{(Mg)^3} 10^{-6} = -6.362 \times 10^{-7} f(\lambda) \tag{19}$$

and

- e_s is the water-vapor pressure at ranging site (mbar),
- P_s is the surface pressure at ranging site (mbar),
- T_s is the surface temperature at ranging site (K),
- θ is the colatitude of ranging site,
- H is the altitude of ranging site above sea level (km),
- M = 28.966 and is the molecular weight of dry air,
- R = 8314.36 J $(\mathrm{K})^{-1}$ $(\mathrm{kg\text{-}mole})^{-1}$ and is the universal gas constant,
- g = 9.784 $\mathrm{m/s^2}$ and is the acceleration of gravity,
- r_0 = 6378 km and is the nominal Earth radius,
- $\boldsymbol{n}$ = $\sin \alpha \boldsymbol{x} + \cos \alpha \boldsymbol{y}$, where $\boldsymbol{x}$ and $\boldsymbol{y}$ are the east and north unit vectors,
- α is the satellite azimuth angle, (α = 0 = North), and
- E is the satellite geometric (unrefracted) elevation angle (Fig. 1.)

Both SC and GC are given in meters when the listed values and units for A, B, C, and D are used and the gradients are in units of reciprocal meters.

The gradient term is a function of the horizontal pressure and temperature gradients and is significant only at the lower elevation angles. Because surface pressure is relatively uniform, under normal conditions, horizontal refractivity gradients will be predominantly a function of the temperature gradients.

The gradient correction is more difficult to calculate than SC because the formula requires measurements of the horizontal pressure and temperature gradients at the ranging site. These gradients can be estimated by measuring pressure and temperature at three or more points surrounding the ranging site. The measurements then can be used to calculate the parameters of an appropriate model for the horizontal variations of P_s and T_s. Such a model depends upon a fixed relationship between the path-averaged gradients and those measured as input data to the model.

B. Spherical Model Accuracy

The accuracy of the spherical correction formula has been extensively checked by Marini and Murray [3] by ray tracing through atmospheric refractivity profiles which were calculated from radiosonde data. The radiosonde data, which consists of P, T, and RH measurements taken at various altitudes during the balloon's ascent, were used to construct spherically symmetric refractivity profiles above the balloon's release point.

The ray-trace corrections and formula showed very good agreement even at low elevation angles. Table I summa-

TABLE I
RANGE ERROR CALCULATED BY MARINI AND MURRAY [3] FOR A RUBY LASER (λ = 694 nm)
(RT_1 is the ray-trace correction for spherically symmetric refractivity profiles.)

Elevation angle	RT_1 Mean (m)	RT_1 - SC Mean (cm)	RT_1 - SC Standard deviation (cm)
80°	2.47	0.07	0.04
40°	3.69	-0.10	0.07
20°	6.91	-0.05	0.12
15°	9.08	0.05	0.19
10°	13.32	-0.08	0.49

rizes Marini and Murray's results for comparisons with 534 different ray traces through refractivity profiles generated from radiosonde observations taken near Dulles Airport, Virginia, during 1967. Additional data from other sites representing all seasons of the year yielded similar results. These results show that the formula for SC is a nearly unbiased estimator of the spherically symmetric ray-trace correction RT_1.

The standard deviation of the difference between SC and RT_1 arises both from modeling errors in the formula for SC and errors in the measured values of P, T, and RH which are used to calculate SC. The dominant error source is pressure. A 1-mbar error in P introduces approximately 14-mm error in SC at 10° elevation.

The effects of input measurement errors on SC can be estimated by taking the partial derivatives of SC with respect to the meteorological parameters. If the measurements of P, T, and RH are assumed to be statistically independent,[1] the total rms error in SC can be expressed as

$$\sigma_{SC} = \left[\left(\frac{\partial SC}{\partial P}\sigma_P\right)^2 + \left(\frac{\partial SC}{\partial T}\sigma_T\right)^2 + \left(\frac{\partial SC}{\partial \mathrm{RH}}\sigma_{\mathrm{RH}}\right)^2\right]^{1/2} \quad (20)$$

where

$$\frac{\partial SC}{\partial P} \simeq \frac{f(\lambda)}{F(\theta, H)}\frac{0.2357}{\sin E} \quad \text{(cm/mbar)} \quad (21)$$

$$\frac{\partial SC}{\partial T} \simeq -\frac{f(\lambda)\ 1.084 \times 10^{-6} P_s K_s}{\sin^3 E} \quad \text{(cm/K)} \quad (22)$$

$$\frac{\partial SC}{\partial \mathrm{RH}} \simeq \frac{f(\lambda)}{F(\theta, H)}\frac{8.615 \times 10^8}{\sin E} \cdot \exp\left\{\frac{17.27(T_s - 273.15)}{237.15 + (T_s - 273.15)}\right\} \quad \text{(cm/percent)} \quad (23)$$

and σ_P, σ_T, and σ_{RH} denote the rms errors in P, T, and RH, respectively. These derivatives are plotted versus elevation angle in Fig. 3. For a well-calibrated satellite ranging system, typical measurement errors could be 0.5–1 mbar for P, 0.7–1.5 K for T, and 5–10 percent for RH. Consequently, for such a system operating above 10° elevation angle, the measurement error in pressure is the largest source of error in SC.

[1] This is only an approximation since RH relates the partial pressure of water vapor to T. However, since these errors are much smaller than that due to pressure, the conclusions presented here are still valid.

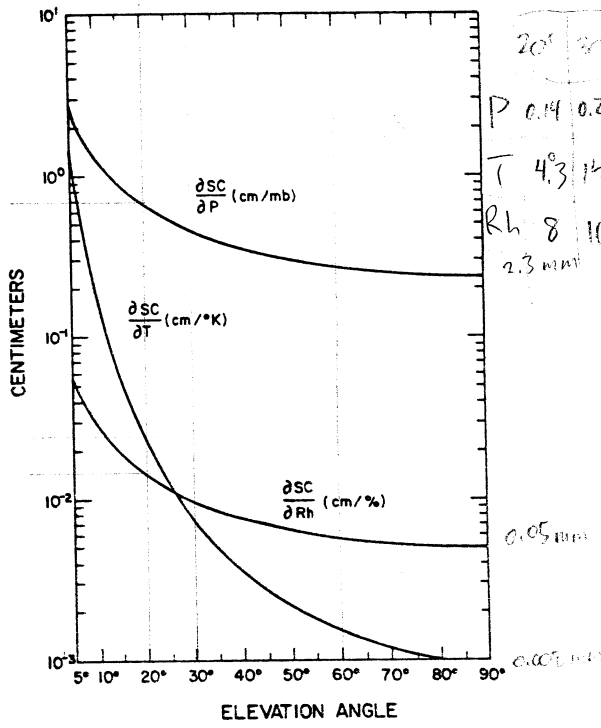

Fig. 3. Variation of the spherical correction formula (7) with respect to pressure, temperature, and relative humidity.

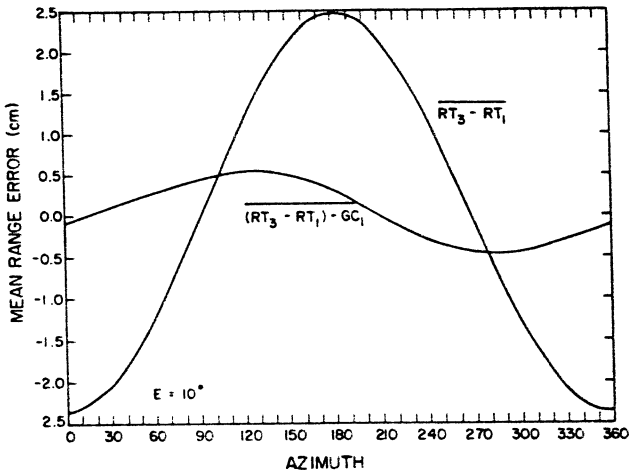

Fig. 4. Mean value of the uncorrected (RT_3-RT_1) and corrected (RT_3-RT_1-GC) gradient error versus azimuth at 10°-elevation angle.

C. Gradient Model Accuracy

The accuracy of the GC formula has also been evaluated by comparing it with ray-trace computations [8]. The results for 10° elevation are illustrated in Fig. 4. RT_3 is the correction obtained by ray tracing through a 3-D refractivity profile calculated from data obtained by radiosondes released almost simultaneously from eight locations near

TABLE II
GRADIENT CORRECTION AND RAY-TRACE COMPARISON: MODEL: $-A \cos(\alpha - \phi)$

Elevation Angle E (deg)	$RT_3 - RT_1$ A (mm)	ϕ (deg)	GC A (mm)	ϕ (deg)	$(RT_3 - RT_1) - GC$ A (mm)	ϕ (deg)
10	24.0	0	22.0	11	4.9	-66
20	6.5	0	6.3	11	1.2	-73
40	1.5	0	1.5	11	0.29	-75
80	0.15	5	0.14	11	0.041	-78

Leonardtown, Maryland, during January and February 1970. The results showed that *GC*, which is a sinusoidal function of azimuth, had a peak-to-peak value of 4–6 cm at 10° elevation and 1–1.5 cm at 20° elevation. They also showed that at 20° elevation angle, the sea-level gradient correction is approximately 1 cm peak to peak for a horizontal temperature gradient of 1°C/100 km. In Fig. 4, RT_1 is the ray-trace correction for the equivalent spherically symmetric refractivity profile. The gradient effects $(RT_3 - RT_1)$ vary sinusoidally with azimuth and are predicted reasonably well by *GC*. The comparisons at 10°, 20°, 40°, and 80° elevation are summarized in Table II. The amplitudes of the gradient correction predicted by the *GC* formula are within a few percent of the ray-trace values $(RT_3 - RT_1)$. However, the average ray-trace correction peaks at 0° azimuth while *GC* peaks at 11° azimuth.

The results shown in Table II should be interpreted with caution. Refractivity gradients have their greatest influence at the higher altitudes, where the laser-beam trajectory is relatively far down range from the laser site. The gradient-correction formula attempts to predict the effects of these high-altitude gradients from surface measurements of P and T.

Errors can be introduced into the *GC* formula in several ways. Terrain features such as mountains, large bodies of water, and vegetative cover probably have a greater influence on meteorological conditions near the ground than at the higher altitudes. Consequently, these terrain features could sufficiently distort the temperature and pressure fields near the ranging site to cause both amplitude and phase errors in *GC*. Errors in measuring P and T at the surface will also cause errors in *GC*.

Both of these problems can be minimized by using many weather stations to obtain the required meteorological data and distributing them over a large area. This approach has the added advantage of also improving the accuracy of spherical correction. However, studies by Gibbs and Majer [9] and Dunn *et al.* [10] indicate the presence of relatively large temperature variations occurring over short spatial scales (~ 10 km) which may significantly distort the calculated value of *GC*. This problem is likely to be more severe in mountainous terrain where the surrounding weather stations may be at widely differing altitudes. Clearly, more tests of the gradient model are required before its operational accuracy can be assessed.

IV. Atmospheric Turbulence

Atmospheric turbulence causes the optical path length to fluctuate. The turbulence itself is caused by small random fluctuations in P and T along the propagation path. The rms path-length fluctuations caused by turbulence are related to the turbulence spatial power spectrum and the refractive-index structure parameter C_n^2, which varies with altitude and time of day. The mean-square path deviation calculated using the von Karmon spectrum is given by [11]

$$\langle \Delta L^2 \rangle = 3.12 C_{n0}^2 L_0^{5/3} h_{\mathrm{Tur}} / \sin E \qquad (24)$$

where

- ΔL is the path-length deviation,
- C_{n0}^2 is the turbulence structure parameter value at the ranging site,
- L_0 is the outer scale of turbulence,
- h_{Tur} is the atmospheric scale height for turbulence, and
- E is the satellite elevation angle.

For satellite ranging, L_0 and h_{Tur} are on the order of 100 m and 3 km, respectively. Under these conditions, the rms path deviations can be up to a centimeter when the satellite is at low elevation angles (~ 10°) and the turbulence is very strong $C_{n0}^2 \simeq 10^{-13} \mathrm{m}^{-2/3}$. Under most conditions C_{n0}^2 will be much weaker ($< 10^{-15}$ $\mathrm{m}^{-2/3}$) so that the rms deviations will be a few millimeters or less. Two-color ranging systems can partially correct for the random path fluctuations, so that in most cases turbulence effects are negligible [11].

V. Two-Color Laser Ranging

Two-color laser ranging provides an alternative to models for determining the atmospheric correction. The technique is based upon the dispersion in the atmospheric refractivity and was first proposed by Prilepin [12] and later by Binder and Owens [13]. The dispersion causes the optical path length at two different frequencies to differ in proportion to the path integrated atmospheric density. Therefore the difference in optical path length at two laser frequencies can be used to estimate the atmospheric correction.

The correction technique can be expressed by letting L_1 and L_2 denote the optical path lengths measured at wavelengths λ_1 and λ_2, respectively. Then the atmospheric correction at wavelength λ_1 is approximately

$$AC = \gamma(L_2 - L_1) \qquad (25)$$

where

$$\gamma = (n_{g2} - 1)/(n_{g2} - n_{g1}). \qquad (26)$$

Although (25) is accurate at optical frequencies at radio and millimeter wavelengths, the differing water-vapor refractivity can introduce substantial errors. This is because at optical frequencies, water vapor contributes only about 1 percent of N_g.

Water vapor, however, is more dispersive than dry air and can cause errors in two-color SLR systems. This error

TABLE III
ATMOSPHERIC CORRECTION TO DIFFERENTIAL PATH-LENGTH RATIO

λ_1 (nm)	λ_2 (nm)	γ
1064	532	21.1
1064	355	7.45
532	1064	-22.1
532	355	12.1
355	1064	- 8.45
355	532	-13.1

can be estimated by assuming that the water vapor is uniformly distributed in the atmosphere up to its scale height, calculating the number of scale heights the laser beam traverses for a given elevation angle, and then utilizing horizontal path calculations for a path of that length. The results show that under extreme conditions (40°C and 100-percent RH), a 17-percent error in estimating RH results in a 0.6-cm range error at 20° elevation. Under more moderate conditions (15°C and 50-percent RH), an 11-percent error in estimating RH results in a 0.06-cm range error at 20°.

Since this error can be ignored in most cases, (26) can be approximated as

$$\gamma = f(\lambda_1)/\{f(\lambda_2) - f(\lambda_1)\}. \tag{27}$$

In Table III, γ is listed for all pairwise combinations of the fundamental, doubled, and tripled Nd:YAG laser wavelengths. The magnitude of the ratios are slightly different when λ_1 and λ_2 are reversed due to the higher refraction when λ_1 is the shorter wavelength. Because γ is on the order of ten for all wavelength pairs, it is necessary to determine the differential path length $(L_2 - L_1)$ with an accuracy which is approximately ten times greater than the desired accuracy for the atmospheric correction. Therefore centimeter-level atmospheric corrections require millimeter-level measurements of $L_2 - L_1$.

VI. Averaging Two-Color SLR Measurements

The accuracy requirements on the individual two-color measurements can be eased considerably if the results of numerous unbiased measurements are averaged. However, since the atmospheric correction and differential path length both are functions of the satellite azimuth and elevation angles, the satellite position must be taken into account when measurements are averaged. For typical refractivity profiles, the atmospheric correction given by (11)–(13) can be modeled approximately as

$$AC = \frac{\beta_1}{\sin E} + \frac{\beta_2}{\sin^3 E} + \frac{\beta_3 \cos \alpha}{\sin E \tan E} + \frac{\beta_4 \sin \alpha}{\sin E \tan E}. \tag{28}$$

The model coefficients β_1-β_4 can be expressed in terms of meterological parameters by using (12) and (13). Alternatively, they can be calculated by using (25) and (27) to compute AC from measurements of L_2-L_1 taken during the satellite pass. Then the data can be fit to (28) by using a regression analysis. A more accurate value of AC could then be obtained by evaluating the regression curves. However, since this technique utilizes the two-color ranging measurements only to calculate the atmospheric model coefficients, it cannot correct for errors in the functional form of the correction model.

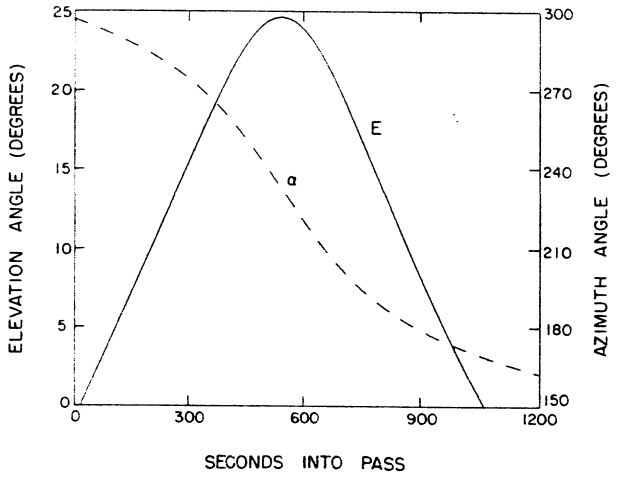

Fig. 5. Azimuth and elevation angle of the Starlette satellite as seen from Greenbelt, Maryland, on July 5, 1979. Zero seconds into the pass is 03.47 GMT.

The performance of the regression model given by (28) has been evaluated using the geometrical parameters of Starlette satellite passes over the Goddard Space Flight Center in Greenbelt, Maryland [14]. The rms error of the regression model can be written as

$$\sigma_{AC} = \frac{\gamma \sigma_{\Delta L}}{N^{1/2}} F \tag{29}$$

where $\sigma_{\Delta L}$ is the rms differential path-length error at zenith, N is the number of two-color measurements made during the satellite pass, and F is a dimensionless error factor which depends on azimuth and elevation angle and on the geometry of the satellite pass. σ_{AC} is proportional to $N^{-1/2}$. This dependence is typical of the error reduction obtained when independent unbiased measurements are averaged. If N is large and F is small, the regression error σ_{AC} will be much smaller than the single measurement error $\sigma_{\Delta L}$.

The azimuth and elevation angle of the Starlette satellite is plotted versus time in Fig. 5 for a typical low elevation angle pass over Greenbelt. Fig. 6 shows the error factor F versus time for this pass. Measurements were assumed to be taken only when the satellite was above 15° elevation. At low elevation angles, the laser pulses are attenuated more than at zenith because of the increased atmospheric scattering. Satellite tracking is also more difficult at low elevations due to the larger satellite distance. This effect was taken into account in calculating the data plotted in Fig. 6 by assuming that $\sigma_{\Delta L} \propto (\sin E)^{\nu}$. ν was chosen so that the path-length error at 20° was 1, 2, 5, and 10 times larger than the error at zenith. These path-length error ratios are denoted as r in the figure.

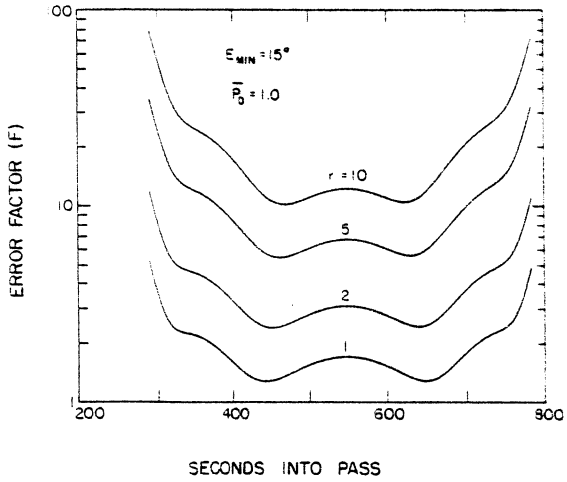

Fig. 6. Error factor for the atmospheric-correction model of (24) and the satellite pass in Fig. 5. The detection probability is one and the minimum elevation angle is 15°. r is the ratio of the differential path length error at 20° elevation to that at zenith.

F is largest at the beginning and end of the pass where the satellite is at the lower angles. The reason for this behavior is evident from (28). The effects of errors in the regression coefficients become more pronounced as the elevation angle decreases, particularly for errors in β_2, β_3, and β_4. Also, the error factor increases at the lower elevation angles where the path-length error is more severe. However, F is usually less than 10 so that if N is large, the regression model will provide a much more accurate estimate of AC than a single two-color measurement. The high elevation-angle Starlette passes showed similar results [14].

As is discussed in the next section, actual two-color measurements are seldom unbiased. Therefore, in practice, the improvement factor due to averaging will only be achieved when the measurement biases are much smaller than the observed atmospheric errors.

VII. Two-Color Laser Ranging Systems

Since two-color ranging was first proposed as a technique to correct for atmospheric refraction, several CW instruments have been built and used for horizontal path measurements. An early instrument [15] used an externally modulated Hg lamp for its optical source, while later instruments [17]–[19] have utilized externally modulated HeNe and HeCd lasers. Length-measurement accuracy with improved instruments [20] is approximately 0.2 ppm.

In principal, CW techniques can also be used to measure or correct for the atmospheric refractivity in SLR. However, several factors make such an approach difficult. The first is the limited optical signal return from the distant satellite. In order to make useful measurements, multiwatt CW lasers are required and must be modulated efficiently at a minimum of several hundred megahertz. The optical receiver must be able to accurately measure the phase difference in the weak CW return signal, without the benefit of range gating. In order to overcome the shot-noise fluctuations of the signal, narrow-band electrical tracking filters must be used in the receiver. These must also track the Doppler shift of the return signals introduced by the moving satellite.

Pulsed multiwavelength systems are becoming attractive alternatives to CW systems for long-distance ranging. Key to their operation is production of picosecond optical pulses of widely separated wavelengths with energies in the tens of millijoules. Presently, the mode-locked frequency-doubled and -tripled ND:YAG laser is a viable commercial candidate. Mode-locked Alexandrite lasers have been reported to produce ~ 10-ps pulsewidths. Frequency-doubled Alexandrite systems operating near 750 and 375 nm would also be well suited for two-color ranging.

Measuring the differential signal delay of photon-limited pulses with millimeter to submillimeter accuracy is the prime technical challenge in pulsed two-color systems. Several pulsed two-color receivers with photomultiplier (PMT) detectors have been built using both a discriminator/time-interval unit-based timing system [21] and a waveform digitizer-based timing system [22]. The PMT-based system [23] built at NASA-Goddard is shown in Fig. 7. Two-color measurements taken with this system over a 921-m round trip horizontal path are shown in Fig. 8. Even though this system is capable of the 1.8-mm accuracy shown in the figure, it requires very careful calibration for accurate use. This is due to the relatively long 500-ps impulse response time of the receiver detectors and electronics. Differential measurements of 1-mm accuracy require timing measurements to within 1 percent of this response time. Although computer processing of the waveform data has given this resolution, the systematic time shifts within detectors and the waveform digitizer must be kept below 1 mm. This difficult requirement makes use of this timing technique unlikely for future two-color SLR applications.

VIII. Streak-Camera Receivers

Streak-camera-based receivers are much more attractive for two-color ranging applications. They use the swept-image converter of the streak camera to provide picosecond response time. Streak cameras are commercially available[2] with 2-ps impulse response time, while developmental streak cameras have 0.2-ps response times [24]. These fast response times are much better matched to mode-locked pulsewidths than are PMT-based receivers.

The operation of a typical linear-scan streak camera is shown in Fig. 9. The incident optical pulse illuminates the photocathode and frees photoelectrons from its rear surface. These are accelerated rapidly by a mesh electrode and then are deflected vertically by a fast electrical sweep. This results in a time-to-space mapping of the electron stream. The resulting electron distribution impinges on the microchannel plate, which preserves the spatial distribution and amplifies it. The amplified electron bundle exits the rear of the plate, and is accelerated into a phosphor screen. This produces a weak optical image whose spatial

[2]For example, Hamamatsu Corp., Model C1370.

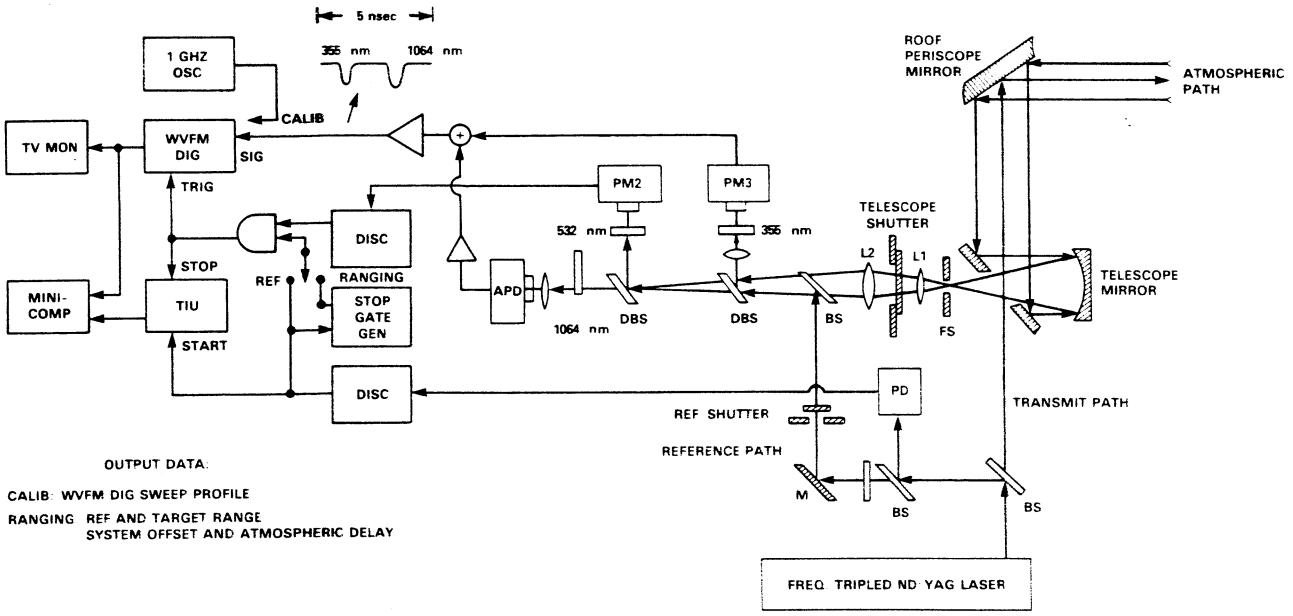

Fig. 7. Three-color ranging system utilizing PMT and APD detectors and waveform digitizer-based timing.

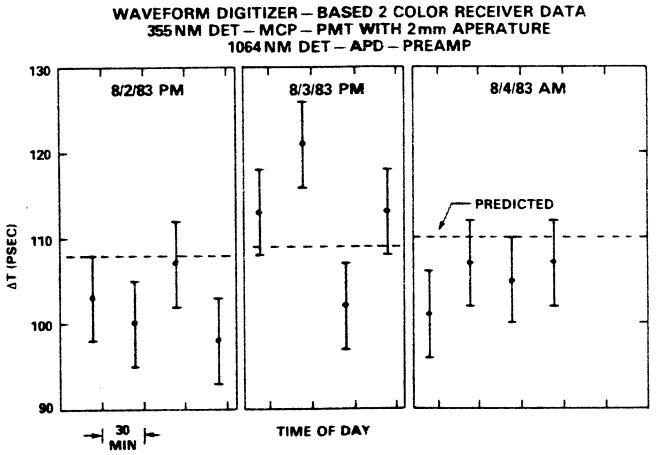

Fig. 8. Three consecutive days of data taken with system shown in Fig. 7. The dashed lines denote the dispersion value predicted from endpoint meterological measurements.

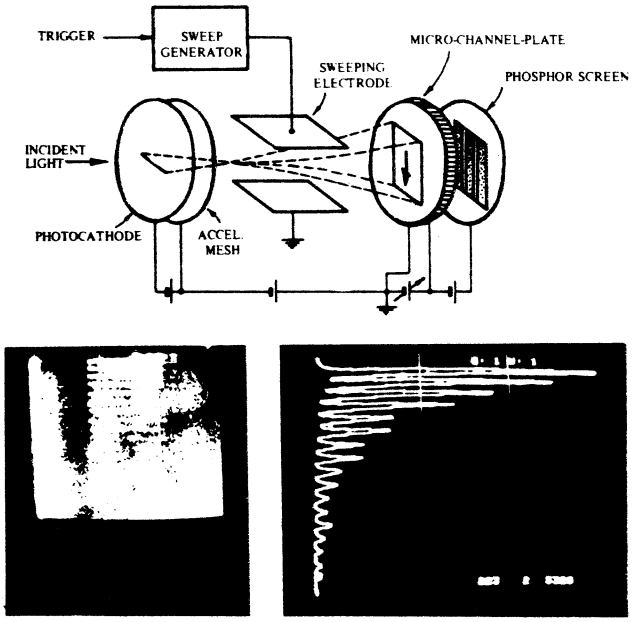

Fig. 9. Operation of a typical linear-scan streak camera. The lower left-hand image is the phosphor screen after the photocathode has been illuminated with a series of exponentially decaying pulses. The lower right-hand is the intensity (horizontal) versus time (vertical) profile of the left-hand image.

intensity distribution is proportional to the temporal intensity distribution of the illuminating optical pulse. In most streak cameras, an intensified video camera reads out this image and a digitizer-microprocessor system converts it back to an intensity versus time profile.

Circular-scan streak cameras have been developed for SLR applications [25]. However, using a dual-channel linear-scan camera permits recording of extended optical return signals in both channels. This allows streak cameras to be used with targets, such as the ocean surface, which are more spatially extended than are retroreflector arrays. Such receivers are useful in other short-pulse laser applications such as altimetry and remote sensing of sea state and atmospheric pressure [26]–[28].

IX. Pulsed Two-Color System Operation

For streak cameras to achieve millimeter-level accuracies in SLR systems, they must be interfaced to the ranging system, possibly modified for near photon limited operation, and carefully calibrated. Abshire *et al.* have recently constructed such a breadboard system at NASA-Goddard and have developed some techniques to meet these requirements [29].

The optical configuration of this system is shown in Fig. 10, and its parameters are summarized in Table IV. This system operates in the following manner. The 30-ps pulses from the dye-mode-locked ND:YAG laser first enter the transmit beam-aligner system, which matches the divergence angles and center points of the 355- and 532-nm

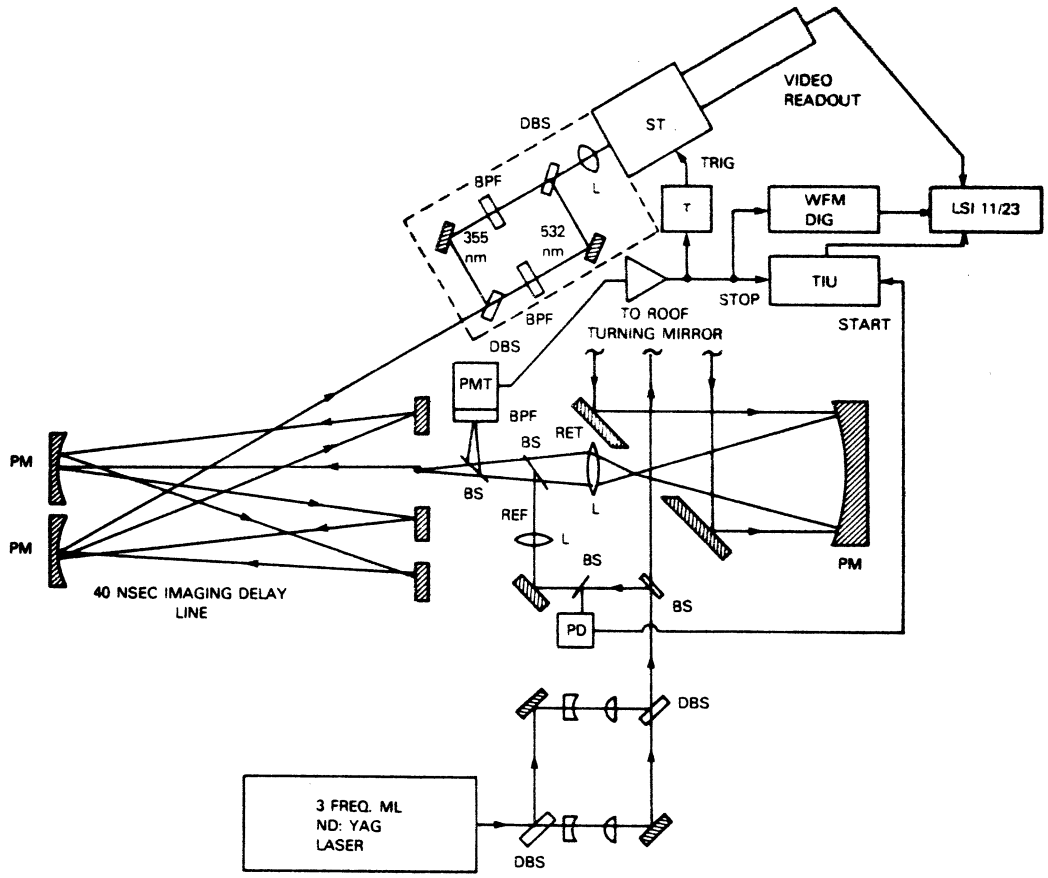

Fig. 10. Current configuration of the streak-camera-based three-color ranging receiver. The roof turning mirror and horizontal path are the same as in Fig. 7.

TABLE IV
PARAMETERS OF STREAK CAMERA-BASED LASER RANGING SYSTEM

LASER	: QUANTEL YG 40: dye ml, 30 psec FWHM 5 mJ @ 1064 nm, 2 mJ @ 532 nm, 1 mJ @ 355 nm DIV: 0.3 TO 1.0 mrad, align: <10% DIV
MIRRORS	: Double dielectric, MAX R @ 355 & 532 nm
τ_{sys}	: Typ 45% AT 532 & 355 nm, (excluding telescope & periscope)
TELESCOPE	: 460 cm^2 AREA, 91 cm FL
PMT	: HAM. R1294, MCP-type, QE ≈ 4%, G ≈ 10^5
WAVEFORM DIGITIZER	: TEKTRONIX R7912
TIU	: HP5370, 100 psec accuracy
STREAK CAMERA	: HAM. 1370, 2 psec resol., 550 psec window, 2.2 psec/chan
MINICOMPUTER	: DEC LSI 11/23, SKYMNK array proc., dual floppy disks

TABLE V
CHARACTERISTICS OF HORIZONTAL PATH FOR RANGING SYSTEM TESTS

LENGTH	: 921.2 m (round-trip)
ELEVATION ANGLE	: +3.5 deg
REFLECTOR	: 2.54 cm CC
END POINT SENSORS	: T — aspirated thermometer P — setra 270 Rh — hair hygrometer
ALGORITHM	: $\Delta T_{32} = \frac{L}{c} \Delta r_{g32} (P_m, T, Rh)$ $L = cT_2 [1 - r_{g2} (P_m, T, Rh)]$ $r_{g\lambda} (P_m, T, Rh) \equiv$ group refractivity at λ (OWENS, APP. OPT., 1967) P_m — midpoint pressure T_2 — TIU reading at λ_2

beams. The original offset is caused by the angle-tuned KD*P doubler and tripler inside the laser. The aligned beams then are reflected up into the periscope system, and are directed to the target cube corner by the roof periscope mirror. The optical return from the corner cube is reflected by the roof mirror and is collected by the receiver telescope. It is reimaged by an eyepiece, which relays the focal point to the start of the optical delay system. Just before this point, a beam splitter reflects part of the optical signal into a PMT, whose output is then amplified and triggers the streak camera. The remainder of the energy enters the 40-ns imaging delay line, which operates in the same manner as a White cell. The signal from this system then enters a light-tight enclosure, where the 355-nm pulses are reflected from a dichroic beam splitter while the 532 pulses pass through it. The pulses in each path then pass through a bandpass filter for background light rejection. They are then recombined by a second dichroic and are focused onto the streak-camera photocathode at slightly offset spots.

The characteristics of the horizontal path, which is currently used for 2-color ranging tests, are summarized in Table V. Equation (5) is used to predict the refractive delay difference between the 532- and 355-nm pulses. The me-

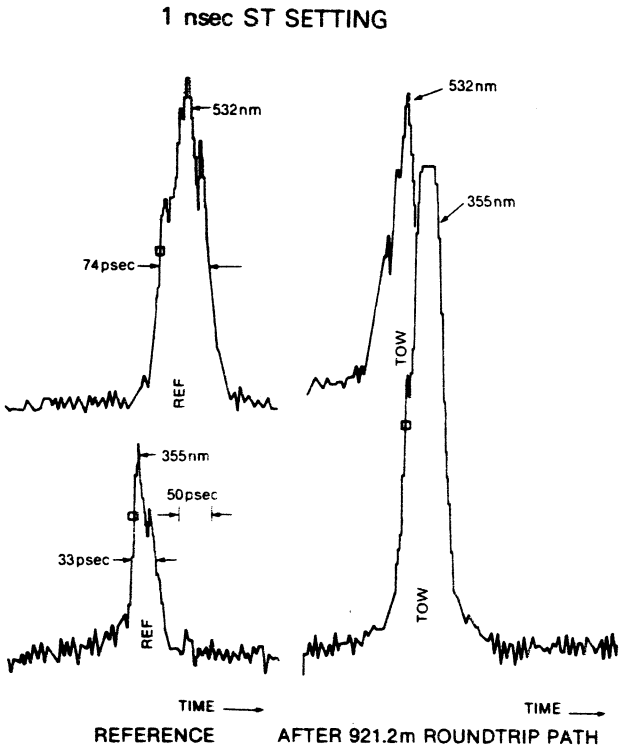

Fig. 11. Laser pulse profiles at 355 and 532 nm taken with the streak-camera receiver: (a) recorded from the reference path, and (b) recorded after the pulses traversed the atmospheric path.

eorological data for this formula are taken from P, T, and RH sensors mounted at the periscope mirror. Sensor accuracy is sufficient to allow less than 1-ps uncertainty in differential delay over this short path.

Laser pulse shapes recorded by the system when the laser etalon is in the 60-ps setting are shown in Fig. 11(a) and (b). Fig 11(a) pulses were recorded from the reference path, while Fig. 11(b) pulses were recorded after a second pulse pair traversed the horizontal path. The pulses are correctly aligned in time for both figures. The shift of the 355-nm pulse in the Fig. 11(b) is caused by the additional refractive delay it encounters in the path. The small scale structure within the pulses shows the picosecond temporal resolution capability of the streak-camera system.

To accurately calculate L_2-L_1, a minicomputer is used to process the streak-camera data. A typical output of the computer program used for dispersion measurements is shown in Fig. 12. Recorded waveforms at 532 and 355 nm are shown on the left-hand side, while the convolution of the two is shown at the top right. For every laser firing, the program selects the convolution peak as its best estimate of L_2-L_1. The bottom figure right shows the histogram of the L_2-L_1 values. The mean and standard deviation of L_2-L_1 are calculated from this histogram. For the data set shown, one channel corresponds to 2.2 ps.

To achieve picosecond-level timing, the nonlinearities in streak-camera sweep must be accurately calibrated. These are measured by inserting a lossy etalon into the reference path, as is shown in Fig. 13. A single pulse input into the etalon results in a train of pulses with exponentially decaying intensities, which are separated by the etalon round-trip time. Since this time is accurately known by the setting of the translation stage, the emitting pulses can be used as temporal calibration markers. The results of this procedure are shown in Fig. 14. Each point plotted here is the average of approximately 25 measurements,

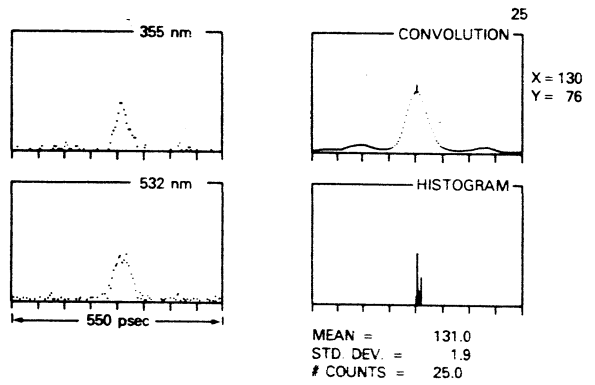

Fig. 12. Computer analysis of streak-camera data illustrating convolution processing to determine differential arrival time.

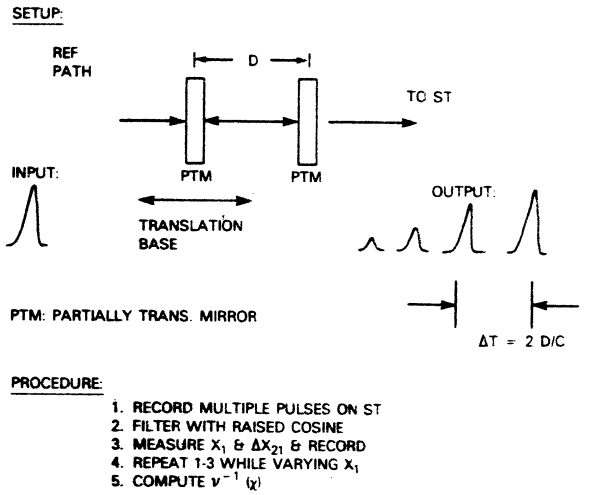

Fig. 13. Procedure used to calibrate the sweep-speed profile of the streak camera.

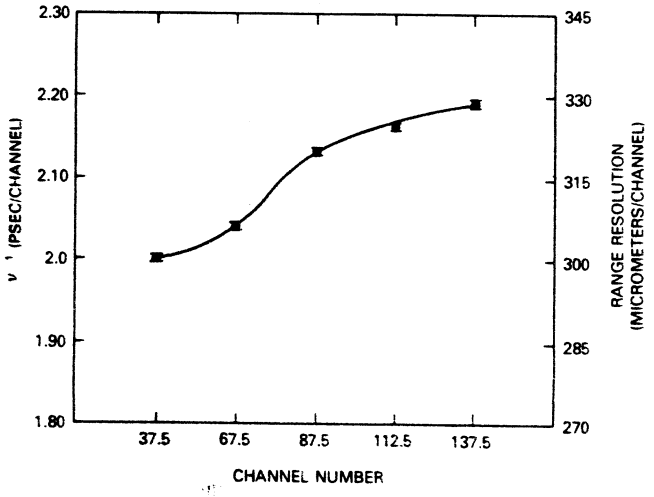

Fig. 14. Sweep-speed profile of our current streak camera, showing 8-percent nonlinearity; sweep-speed calibration: 1-ns scale, 169-ps pulse separation.

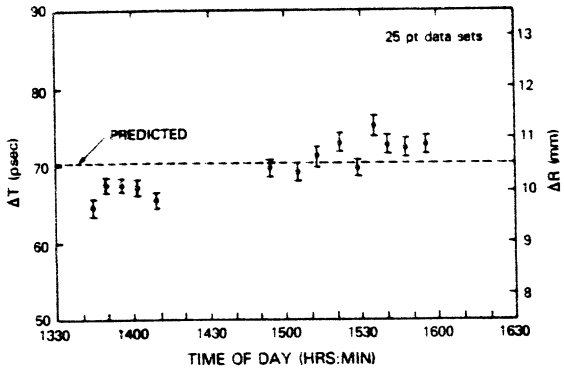

Fig. 15. Two-color ranging results taken with system shown in Fig. 10 over the 921.2-m horizontal path. The error bars denote the single measurement standard deviation. The average system error is 2 ps.

and the error bars are the standard deviation of the sample mean values. The data show that the sweep speed is fastest at the start of the sweep, and slows by ~8 percent over the region shown. This profile is used to compensate subsequent measurements for this effect.

To accurately measure the atmospheric delay, the fixed offsets within the LR system also must be removed. These offsets are primarily due to the transmit and receiver beamsplitter assemblies, where the 532- and 355-nm pulses traverse physically different paths. These offsets are removed by first measuring the differential delay over the horizontal path. Then the laser output is blocked from traversing the path and the reference shutter is opened. The same procedure is then repeated while the laser pulses traverse only the reference path within the instrument. Since all fixed offsets within the system are common to both paths, subtracting the reference values from the path values leaves only differential delay caused by the atmosphere. Therefore the final atmospheric measurement can be expressed as

$$L_2 - L_1 = c\left\{\left[\int_{x_1}^{x_2} v^{-1}(x)\,dx\right]_{\text{ref}} - \left[\int_{x_1}^{x_2} v^{-1}(x)\,dx\right]_{\text{path}}\right\} \quad (30)$$

where x_1 and x_2 are the measured positions of the 355- and 532-nm pulse peaks and $v^{-1}(x)$ is the streak-camera inverse sweep speed. Both the sweep speed and offset corrections are very similar to those developed for the waveform digitizer-based two-color LR system [22], [23], [27].

Recent results [29] from repetitively measuring the atmospheric dispersive delay after using these procedures are shown in Fig. 15. Each plotted point is the mean value of 25 measurements and the error bars show ± one standard deviation. The average bias of the first set of 4 points is −3 ps, while the average bias of the second set of 9 points is 2 ps. The shifts in the average value are thought to be caused by small errors in spatially aligning the reference to the tower path. Even with these errors, the accuracy of L_2-L_1 is within ±0.5 mm for this measurement set. Dual-color SLR data of such accuracy can be used to measure the atmospheric delay of single-color measurements to 0.5 cm.

X. Discussion

Streak-camera-based two-color laser ranging systems are still in the developmental stage. To date development efforts have concentrated upon integrating the streak camera into the laser ranging system and identification and reduction of systematic timing errors. Although the results shown in this paper were taken with the breadboard system operating at high signal levels, no major problems are anticipated when such systems are operating at low return-signal levels. For these tests, an external image intensifier will be used to increase detection sensitivity.

Two-color system accuracy has not yet been determined in SLR tests. The modifications anticipated for a short-pulse MOBLAS-type system to accommodate the two-color system include adding a frequency-tripling crystal to the mode-locked Nd:YAG lasers, changing the intracavity etalon to one for 30-ps pulses, adding a transmit beam aligner to co-align the 532- and 355-nm beams, and replacing transmitter and receiver beam handling mirrors with double-stack dielectric mirrors. This last step is important since, due to lower production efficiency and higher optical and atmospheric losses, pulsed two-color systems are likely to be power limited at the shorter wavelength.

One plan for improving the atmospheric correction for SLR systems is to implement two-color systems initially at only a few representative sites. The targets for these tests could be cube-corner equipped high-altitude aircraft balloons, or the STARLETTE or LAGEOS satellites. The atmospheric corrections measured with these two-color systems can then be compared to that from atmospheric models. Long-term tests should determine the accuracy of the models and could determine if the models can be improved by using perhaps additional meterological data. The results of such tests should be valuable in determining the accuracy level at which two-color systems will be required for atmospheric corrections in operational SLR systems.

Acknowledgment

We would like to thank the reviewers for their helpful suggestions as well as H. E. Rowe and J. F. McGarry for their work on the streak-camera receiver.

References

[1] J. J. Degnan, T. W. Zagwodzki, and H. E. Rowe, "Satellite laser ranging experiments with an upgraded Moblas station," presented at the 5th Int. Workshop on Laser Ranging Instrumentation, Royal Greenwich Observatory, Herstmonceux, England, Sept. 17-21, 1984.

[2] J. C. Owens, "Optical refractive index of air: Dependence on pressure, temperature and composition," *Appl. Opt.*, vol. 6, no. 51, 1967.

[3] J. W. Marini and C. W. Murray, Jr., "Correction of laser range tracking data for atmospheric refraction at elevation angles above 10 degrees," Goddard Space Flight Center, Greenbelt, MD, NASA Tech. Rep. X-591-73-351, 1973.

[4] J. Saastamoinen, "Introduction to practical computation of astronomical refraction," *Bull. Geodesique.*, vol. 107, no. 383, 1972.

[5] J. L. Davis, A. E. E. Rodgers, A. Herring, and I. I. Shapiro, "Geo-

desy by radio interferometry: Calibration of the wet and dry troposphere," *Trans. Amer. Geophys. Union (EOS)*. vol. 65, p. 853, 1984.
[6] R. N. Treuhaft, G. E. Lanyi, and O. J. Sovers, "Emperical troposphere modelling from DNS intercontinental VLBI data," *Trans. Amer. Geophys,. Union (EOS)*, vol. 65, p. 191, 1984.
[7] C. S. Gardner, "Correction of laser tracking data for the effects of horizontal refractivity gradients," *Appl. Opt.*, vol. 16, p. 2427, 1977.
[8] C. S. Gardner, J. R. Rowlett, and B. E. Hendrickson, "Ray tracing evaluation of a technique for correcting the refraction errors in satellite tracking data," *Appl. Opt.*, vol. 17, p. 3143, 1978.
[9] B. P. Gibbs and V. Majer, "Accuracy assessment of the atmospheric correction used in the NASA laser ranging program," Business & Techn. Sys., Seabrook, MD, Tech. Rep. BTS-FR-81-166. Sept. 1981.
[10] P. Dunn, W. Pearce, and K. Borman, "The effects of atmospheric refraction in laser ranging measurements," in *Proc. General Meeting Int. Assoc. Geodesy* (Tokyo, Japan), May 7-15, 1984.
[11] C. S. Gardner, "Effects of random path fluctuations on the accuracy of laser ranging systems," *Appl. Opt.*, vol. 15, p. 2539, 1976.
[12] M. T. Prilepin, "Light modulating method for determining average index of refraction of air along a line," *Tr. Tsent. Nauchne., Issled. Inst. Geod., Aerol. i Kartog.*, vol. 127, pp. 114, 127, 1957.
[13] P. L. Bender and J. C. Owens, "Correction of optical distance measurements for the fluctuating atmospheric index of refraction," *J. Geophys. Res.*, vol. 70, p. 2461, 1965.
[14] C. S. Gardner and R. A. Axford, Jr., "Regression models for multicolor satellite laser ranging," Radio Research Lab, Univ. of Illinois, Urbana, Tech. Rep. 505, Mar. 1980.
[15] M. C. Thompson and L. E. Wood, "The use of atmospheric dispersion for the refractive index correction of optical distance measurements," in *Proc. Int. Assn. Geodesy Symp. Electronic Distance Measurement* (Oxford, England), Sept. 1965.
[16] J. C. Owens, "The use of atmospheric dispersion in optical distance measurement," *Bull. Geodesique*, vol. 277, no. 89, 1968.
[17] K. B. Earnshaw and J. C. Owens, "A dual wavelength optical distance measuring instrument which corrects for air density," *IEEE J. Quantum Electron.*, vol. QE-3, p. 544, 1970.
[18] K. B. Earnshaw and E. N. Herdandez, "Two-laser optical distance measuring instrument that corrects for the atmospheric index of refraction," *Appl. Opt.*, vol. 11, p. 749, 1972.
[19] L. E. Slater and G. R. Huggett, "A multiwavelength distance measuring instrument for geophysical experiments," *J. Geophys. Res.*, vol. 81, p. 6299, 1976.
[20] G. M. B. Bouricius and K. B. Earnshaw, "Results of field testing a two-wavelength optical distance measuring instrument," *J. Geophys. Res.*, vol. 79, p. 3015, 1974.
[21] B. Querzola, "High accuracy distance measurement by two-wavelength pulsed laser sources," *Appl. Opt.*, vol. 18, p. 3035, 1979.
[22] J. B. Abshire, "Pulsed multiwavelength laser ranging system for measuring atmospheric delay," *Appl. Opt.*, vol. 19, p. 3436, 1980.
[23] J. B. Abshire, "Pulsed multiwavelength laser ranging system," NASA Tech. Memo. 83917, Greenbelt, MD, Mar. 1982.
[24] W. Sibbett, H. Niu, M. R. Boggs, "Femptosecond streak image tube," in *Proc. 15th Int. Congress High-Speed Photography and Photonics* (San Diego, CA), p. 271, Aug. 1982.
[25] C. B. Johnson, S. Kevin, J. Bebris, and J. B. Abshire, "Circular-scan streak tube with solid state readout," *Appl. Opt.*, vol. 19, p. 3491, 1980.
[26] C. S. Gardner, B. M. Tsai, and K. E. Im, "Multicolor laser altimeter for barometric measurements over the ocean: Theoretical," *Appl. Opt.*, vol. 22, p. 2571, 1983.
[27] J. B. Abshire and J. E. Kalshoven, Jr., "Multicolor laser altimeter for barometric measurements over the ocean: Experimental," *Appl. Opt.*, vol. 22, p. 2578, 1983.
[28] J. B. Abshire, J. F. McGarry, B. M. Tsai, and C. S. Gardner, "Correlation measurements of the ocean surface reflections when using a modelocked multiple wavelength Nd:YAG transmitter," in *Conf. Lasers and Electro-Optics* (Anaheim CA), paper WL2, June 1984.
[29] J. B. Abshire, J. F. McGarry, H. E. Rowe, and J. J. Degnan, "Streak camera-based laser ranging receiver development," presented at the 5th Int. Workshop Laser Ranging Instrumentation, Royal Greenwich Observatory, Herstmonceux England, Sept. 17-21, 1984.

*

James B. Abshire (S'73-M'81-SM'85) was born in Knoxville, TN, on December 6, 1951. He received the B.S. degree in electrical engineering from the University of Tennessee, Knoxville, in 1974 and the M.S. and Ph.D. degrees in electrical engineering from the University of Maryland, College Park, in 1978 and 1982, respectively.

He joined the NASA-Goddard Space Flight Center, Greenbelt, MD, as a co-op student in 1971 and as a full time employee in 1974. Since that time he has done research on high-speed photomultipliers, satellite retroreflector array evaluation, spaceborne and airborne laser ranging systems, two-color laser ranging, laser altimetry, and laser communications. His current research interests are in developing submillimeter accuracy laser systems for geodetic and remote sensing applications, and in free-space laser communication systems.

Dr. Abshire is a member of Tau Beta Pi, Eta Kappa Nu, and the Optical Society of America.

*

Chester S. Gardner (S'72-M'73-SM'78) was born in Jamaica, NY, on March 29, 1947. He received the B.S. degree from Michigan State University, East Lansing, in 1969 and the M.S. and Ph.D. degrees in electrical engineering from Northwestern University, Evanston, IL, in 1971 and 1973, respectively.

From 1969 through 1971, he was a member of the technical staff at Bell Telephone Laboratories, Naperville, IL, working on the development of No. 4 ESS. He was a Walter P. Murphy Fellow at Northwestern University from 1971 to 1973. In 1973, he joined the faculty of the University of Illinois, Urbana-Champaign, where he is currently Professor of Electrical and Computer Engineering, Director of the Electro-Optic Systems Laboratory, and a Beckman Associate in the Center for Advanced Study. His research interests include optical communications, lidar, laser ranging, image processing, and spread spectrum communications.

Dr. Gardner is a Fellow of the Optical Society of America and a member of Tau Beta Pi, Eta Kappa Nu and Sigma Xi. He has served as IEEE Region 4 Technical Activities Chairman and as chairman of the Central Illinois Section of the IEEE.